Stable Photoelectrochemical Hydrogen Evolution for 1000 h at 14% Efficiency in a Monolithic Vapor-fed Device

Journal of The Electrochemical Society, 2020 **167** 066502

Stable Photoelectrochemical Hydrogen Evolution for 1000 h at 14% Efficiency in a Monolithic Vapor-fed Device

Tobias A. Kistler,[1,2,3] Min Young Um,[1,2] and Peter Agbo[1,2,z]

[1]*Chemical Sciences Division, Lawrence Berkeley National Laboratory, Berkeley, California, United States of America*
[2]*Joint Center for Artificial Photosynthesis, Lawrence Berkeley National Laboratory, Berkeley, California, United States of America*
[3]*Walter Schottky Institute and Physics Department, Technische Universität München, Garching, Germany*

This report builds on our recent disclosure of a fully-integrated, photoelectrochemical (PEC) device for hydrogen evolution using a structure incorporating a III–V triple-junction photovoltaic (PV) embedded in a Nafion membrane. Catalyst integration is realized by compression of catalyst-modified, carbon electrodes against the front and back PV contacts, resulting in a wireless, monolithic PEC assembly. Using this device architecture, we demonstrate significant enhancements in device stability and longevity, by transitioning from a liquid-water to water-vapor anode. Our use of a gas-fed anode enables 1000 h of cumulative device operation at a peak solar-to-hydrogen efficiency of 14%, during simulated, solar illumination at 1 sun and outdoor, diurnal cycling. Vapor-fed water oxidation is shown to reduce drops in device performance by mitigating the corrosion effects that are commonly associated with full-aqueous immersion of the electrochemical and photovoltaic elements in PEC devices.
 [DOI: 10.1149/1945-7111/ab7d93]

Manuscript submitted November 14, 2019; revised manuscript received January 24, 2020. Published March 19, 2020.

Supplementary material for this article is available online

Photoelectrochemical (PEC) water splitting is one of the most promising technologies for renewable and clean hydrogen production.[1–3] Numerous, photoelectrochemical devices for solar-driven water splitting have been reported recently, reaching record efficiencies of 19% in monolithic architectures.[4–6] However, those liquid-fed devices are generally not stable enough to be considered for commercial applications, degrading significantly within hours or even minutes, due to the harsh acidic or basic chemical environments in which such PEC devices commonly operate. It is expected that a water vapor feed can increase the stability of such a device significantly, due to the milder environment for the PV.[7] For conventional electrolyzers, which operate at higher current densities in the range of 1–2 A cm^{-2}, a water vapor feed is problematic because of the resulting reactant mass transport limitations at the anode. However, solar-driven electrolyzers are generally limited by the current density that the PV can supply, normally in the range of 10–20 mA cm^{-2} unless the light is concentrated,[8] opening the door for vapor-fed, PEC devices.[9] Furthermore, bubbles forming in front of the PV can attenuate the incident light intensity, lowering the PV's photocurrent, while bubbles forming in between the water and the electrocatalysts reduce the reactant-catalyst contact area, decreasing the electrochemical performance.[9–13] Finally, water vapor operation obviates any need for a liquid pump, while minimizing the risk of freezing and membrane or electrode poisoning caused by impurities that may be found in liquid water.[13–16] Vapor-fed, solar hydrogen devices have shown promising results, with anodes fed by ambient air[13] or seawater vapor,[16] reaching solar-to-hydrogen (STH) efficiencies as high as 15%.[17] While the latter device uses earth-abundant catalysts, their demonstrated efficiencies were not sufficiently stable, with degradation visible during the first 24 h of operation and rather high input flow rates of 230 ml min^{-1} were used. In this report, we demonstrate an integrated, wireless device structure operated by a humidified nitrogen feed at a flow rate of 5 sccm. The device operation was stable for more than 1000 h, with only minor, irreversible PV degradation visible, setting a benchmark for PEC device stability.

Experimental

The III–V triple-junction PV and iridium/platinum catalysts on carbon paper used for this study, as well as the integration of the PV into the Nafion membrane, have been described previously in detail by the authors.[18] The front of the PV was coated with a transparent epoxy, serving as both anti-reflective[18] and protective coating.[7,19] Furthermore, the same solar simulator and reference cell were used, indicating an illumination error of less than 1%, due to the bandgap mismatch between the reference cell and the triple-junction PV.[18] However, the carbon paper was coated with catalysts only on the side facing the membrane for this study.

Structure of the device.—For water vapor operation, it is essential to reduce the distance for ion transport and minimize dead volumes to prevent large losses due to resistive effects.[20–23] Therefore, we modified the supporting structure used for the liquid water-fed system[18] and created a more compact device design (Fig. 1). The endplates were machined from acrylic material (PMMA) which both incorporate two flow ports each, and 0.1 mm deep flow channels resulting in a channel volume of roughly 18 mm^3. The gases flow from the bottom of the cell through the flow channels to the top and can diffuse through the carbon paper gas diffusion layers (GDLs). Silicone gaskets were used to seal the cell (C and G in Fig. 1) and to reduce the condensation of water vapor at the PV front (B in Fig. 1). At the center of the PEC device lies the PV-integrated membrane (PIM) structure, with one catalyst-coated, carbon paper being compressed against each side. The PV size is 1 cm^2 and equals the catalyst-deposited area of the carbon paper (silver color on GDL in Fig. 1).

Generally, current measurement is not possible in monolithic PEC cells.[24] However, due to the removable insulation layer between the PV front contact and the cathode catalyst support, the electrons can be rerouted through a potentiostat before they react with protons to form hydrogen. When this shunt path is removed, the device can operate monolithically, without wires.[18] Additionally, the voltage provided by the PV during full PEC cell operation can be measured by connecting one lead to the PV front and back contact each. As voltage and current are concurrently monitored in real time, the operating point of the PEC cell can be determined precisely throughout an experiment, enabling real-time separation of photovoltaic and catalytic current losses.[25]

[z]E-mail: pagbo@lbl.gov

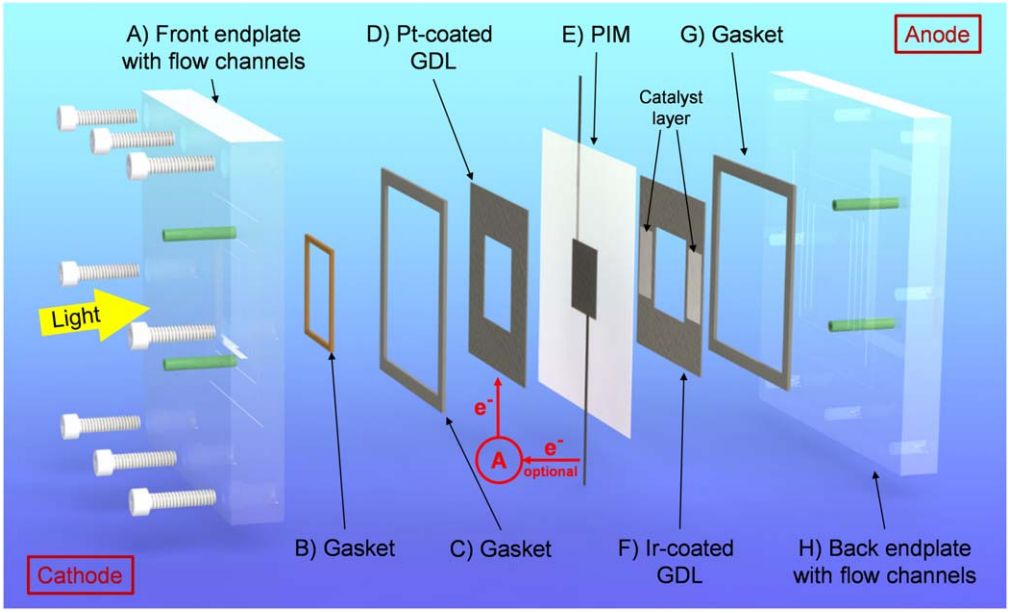

Figure 1. A full assembly diagram of the monolithically-integrated, photoelectrochemical device, using an optional shunt path as an instrument for monitoring device current and faradaic efficiency, by rerouting electrons collected from the PV front through a potentiostat, before finally reacting with protons at the cathode catalyst layer.[18]

Lab conditions.—During the indoor lab tests, the PEC cell was illuminated by a solar simulator providing an illumination intensity of 1 sun (0.1 W cm^{-2}). High purity nitrogen flowed through a heated (70 °C if not otherwise mentioned) bubble humidifier, filled with Milli-Q water (resistivity $>$ 18.2 MΩ*cm), at a flow rate of 5 sccm, and then through the anode side of the cell. The cathode was purged by a dry nitrogen flow at 10 sccm. Current-voltage curves were taken at different scan rates to measure the electrochemical (20 mV s^{-1}) as well as the photovoltaic (200 mV s^{-1}) performance.

On-sun conditions.—For the outdoor, on-sun tests, the PEC cell was mounted, side by side with a monocrystalline silicon reference cell,[18] on a 2-axis, solar tracker system (STR-22G Sun Tracker from EKO Instruments, Japan). The solar tracker uses both GPS co-ordinates and an optical sensor to track the sun's position precisely. As the solar tracker moves, the position of the PEC cell moves from an almost vertical position in the mornings and evenings to a nearly horizontal position during midday. Due to this movement, the tubing connecting the cell to the humidifier as well as the electrical leads need to be longer as their ends are fixed on the ground. The longer tubing leads to increased response times if measurement conditions such as the bubble humidifier temperature need to be adjusted. The carrier gas flow rates were chosen according to the flow rates used in the lab, however, the outlets of the PEC cell were not connected to a gas chromatograph (GC). As a result, the cell was not pressurized due to backpressure from the GC. Furthermore, the air temperature and relative humidity change according to the weather conditions, which were monitored by a weather station at Lawrence Berkeley National Laboratory. The data from the station is available online via the websites of the National Oceanographic and Atmospheric Administration's (NOAA) National Weather Service or the University of Utah, and is reported together with the outdoor testing results.

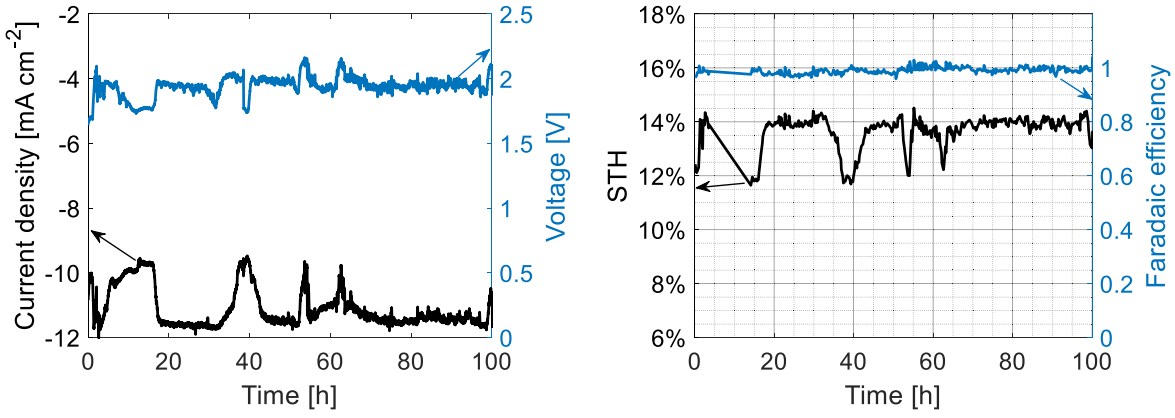

Figure 2. First 100 h of the 188-hour stability test (a) Current-voltage data during this trial. Local maxima of the voltage mark a high overpotential for the water splitting reaction due to membrane dehydration, while decreased currents at low voltages indicate losses caused by condensation of water at the PV front. (b) The faradaic efficiency is constant near 1 during this test, while the solar-to-hydrogen (STH) efficiency follows the current fluctuations. Between hours 4 and 14, GC data was not available and the efficiency data was interpolated during that time period.

Results

Different feed conditions were examined without the use of a PV, in a mockup cell driven by a potentiostat (Fig. S1 is available online at stacks.iop.org/JES/167/066502/mmedia). The solar-to-hydrogen (STH) efficiency as well as the current density results presented in this section are based on the photo-active, illuminated area of the PV (1 cm^2). The hourly time axis is sequential in between different figures, with some experiments shown in the Supplemental Material.

Stability test in the lab.—We tested the vapor-fed system for stability, beginning with a 188-hour trial. The current-voltage data and the efficiency values during the first 100 h are displayed in Fig. 2, while the full 188-hour test is shown in Fig. S2, including the product stoichiometry and the polarization curves before and after this trial. Concurrent voltage and current density data (Fig. 2a) allows tracking of the operating point, with the voltage describing the overpotential needed for the electrochemical reactions at a given current density.[25] The device shows remarkable stability, with a minimum STH efficiency of 12%, peaking at 14%, while the faradaic efficiency is constant near 1 (Fig. 2b). After this 188-hour test, the cell was allowed to rest for one hour and then tested again for 24 h (Fig. S3), confirming the absence of irreversible degradation.

Outdoor, on-sun test.—Following the simulated, diurnal test shown in Fig. S4, the device was tested outdoors on the roof, directly illuminated by the sun, keeping the gas flow rates the same as indoors. The IV-curves of the PV look very similar comparing indoor and outdoor operation during peak illumination (Fig. S5a), confirming that the simulated lab conditions are comparable to the outdoor conditions. However, the illumination intensity is not constant and other environmental conditions such as the temperature and relative humidity fluctuate considerably. The illumination intensity was recorded with a reference cell and peaked around 1.04 suns with no clouds visible at the sky throughout this 98-hour test, confirmed by data from a weather station (Fig. S5b). The higher illumination intensity measured by the reference cell (Fig. 3b) compared to the weather station is caused by reflection from elements on the roof such as walls and pipes. The recorded current and voltage values shown in Fig. 3a fluctuate with the light intensity, with no current being measured during the dark cycles, except for a few minutes during the last hour of the dark cycle. The solar tracker was positioned on a roof and while one wall blocked most of the light from the east side during the first hour after sunrise, there is a small opening in that wall permitting illumination for about 25 min. At the beginning of the illuminated cycles, the current increases quickly as the illumination intensity is already above 0.9 suns at that time (Fig. 3b). The hydration conditions of the PEC cell were more difficult to control during this outdoor test, caused by varying temperature, relative humidity, pressure, tilt angle of the cell and longer tubing resulting in increased response times. Therefore, the current and voltage fluctuate considerably more compared to the indoor test, as it was not straightforward to find the optimum point which balances dehydration of the membrane and condensation of water at the PV front. For this trial, the GC was not available and therefore, the faradaic efficiency was assumed to be the same as indoors (~98%). Using this assumption, the resulting STH efficiency during outdoor testing is plotted in Fig. 3b, with a minimum of 11% and a maximum efficiency of 14% being reached during the last two cycles.

The authors note that the solar tracker was turned off during the first dark cycle, making the PEC cell face west during that time. This resulted in increased illumination between 0.1 and 0.2 suns (Fig. 3b) by reflection of walls and pipes on the roof during the last 2 h of the first dark cycle, leading to an increased current being measured during this time.

Second stability test in the lab under optimized operating conditions.—After the outdoor test, the PEC cell was dismantled, keeping all active components the same but only swapping one gasket for a thinner one, to increase the compression of the carbon paper against the membrane and seal the PV front better from the environment. This resulted in an initial operating point near 12 mA and 1.65 V determined from the intersection point of the electrochemical (EC) and PV IV-curves (Fig. 4a). We note, the somewhat increased short circuit current of the PV, compared to the current measured during the first trial (Fig. S2a), is likely caused by a slightly different angle of the PV in the assembly or the assembly towards the solar simulator.

The current-voltage data during this 180-hour trial is shown in Fig. 4b. At the beginning, the bubble humidifier was not heated, resulting in a slowly decreasing current due to membrane dehydration. At hour 323, the heater of the bubble humidifier was set to the same temperature (70 °C) as during the previous indoor tests, followed by 75 °C at 336 h, reducing the membrane resistance and increasing the current. During the last 160 h, the current was mostly stable, decreasing by roughly 0.3 mA during this time, the result of a decreased PV fill factor, as shown in the inset of Fig. 4a. The stable current results in a remarkably constant STH efficiency near 14% throughout this 180-hour test, with faradaic efficiencies for hydrogen

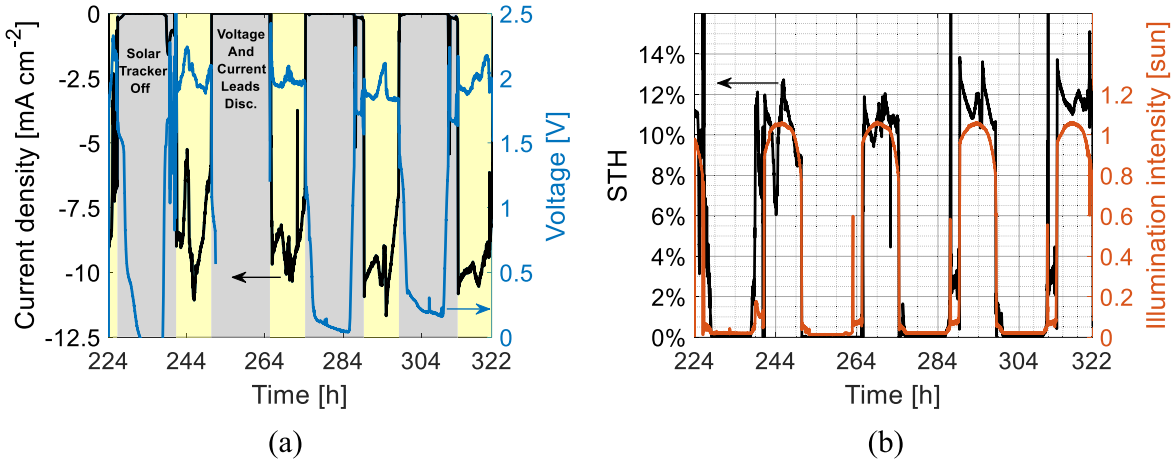

Figure 3. Outdoor testing (a) Current-voltage tracking during this trial shows the fluctuating current and voltage due to changing illumination and hydration conditions. The grey background marks the dark time periods, with negligible light reaching the PEC cell, while the yellow background marks the illuminated time periods. During the first dark cycle, the solar tracker was turned off and during the second dark cycle, the voltage and current leads were disconnected from the PEC cell. (b) STH efficiency and illumination intensity, including effective light concentration effects from reflective roof elements, resulting in temporary intensities above 1 sun.

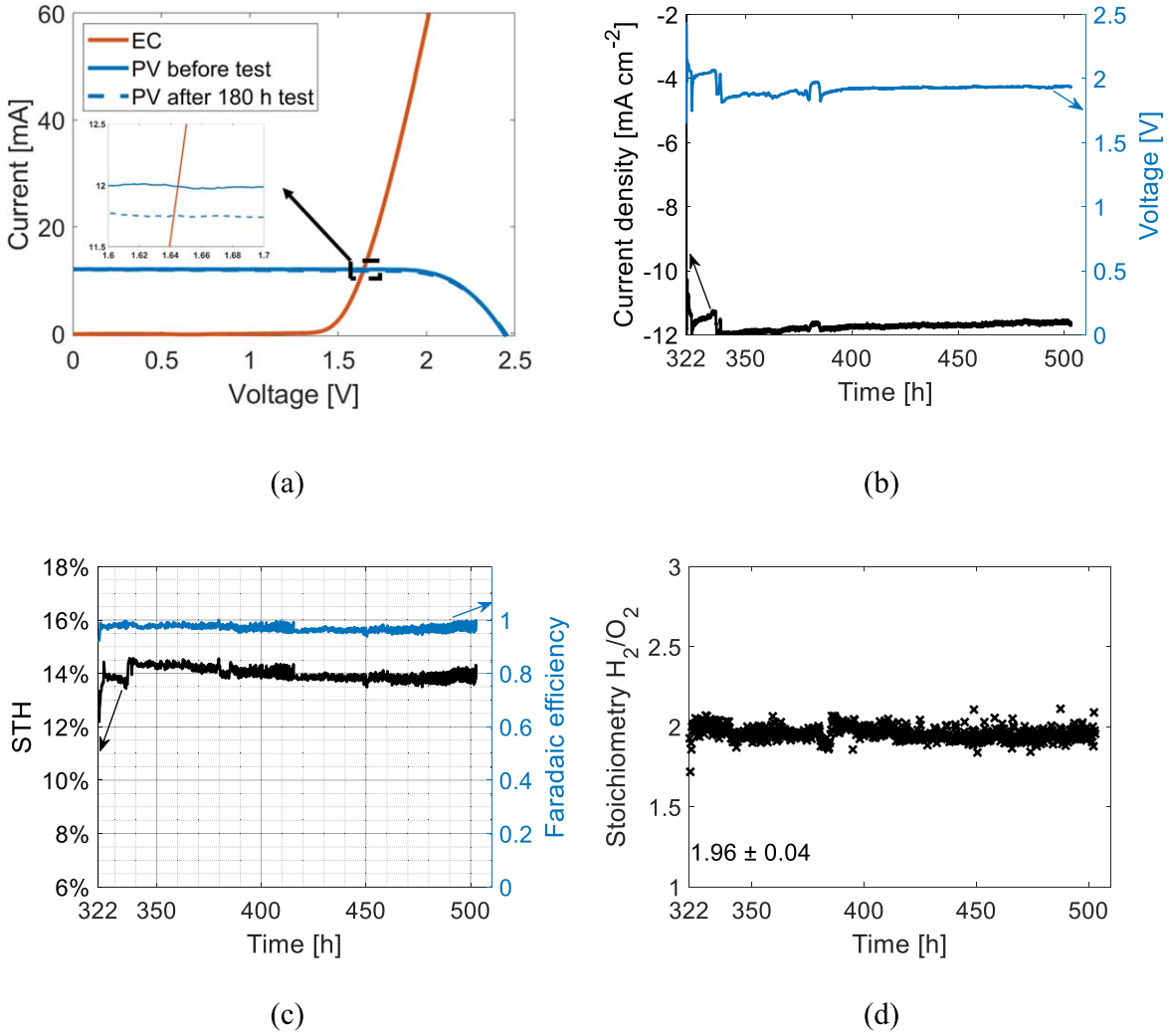

Figure 4. 180-hour stability test (a) The intersection of the polarization curves, corresponding to the electrochemical (EC) and photovoltaic (PV) performance, yield the expected operating point of the PEC device. The PV load curve shows a decreased fill factor after the 180-hour trial from an initial value of 0.79 to a final value of 0.77, reducing the current at the operating point by roughly 0.3 mA. (b) Current-voltage measurements during the full 180 h of operation. (c) Solar-to-hydrogen and faradaic efficiency. (d) The product stoichiometry remained constant around 1.96 ± 0.04 during the whole experiment.

generation close to 1 (Fig. 4c). Furthermore, the product stoichiometry of hydrogen and oxygen remains steady near the expected value of 2, as evidenced by gas chromatography (Fig. 4d). After the improved, indoor stability test, the PIM device continued to operate on-sun, extending the cumulative device operation time beyond 1000 h (Fig. S6). The reference cell was removed from the solar tracker for this long-term test, and the effective illumination intensity was calculated from the solar position and weather station data (Fig. S7).

Discussion

During the course of the first 500 h of testing, the PIM device only displays minor, irreversible current losses of 0.3 mA or 2.5% compared to its initial current, followed by a stable, outdoor performance for about one month. A 2% drop in the PV fill factor is responsible for this current reduction, while there were no indicators for electrocatalytic degradation. The lower PV performance can be caused by an increasing contact resistance, which is part of the series resistance. Due to the increased compression during the last 180 h of indoor operation, the contacts could have degraded if pressurized unfavorably. Generally, a higher compression of the PEC cell risks damage to the fragile PV, while enhancing the contact between the Nafion membrane and electrocatalysts. Thinner gaskets also allowed slightly higher humidification temperatures as the PV was sealed better from the cathode flow channels, reducing the chances of vapor water condensing at the PV front, while increasing the hydration of the Nafion membrane. Overall, a tighter compression of the cell components enabled more stable device operation. Alternatively, components such as zeolites[13] or silica fillers and heteropolyacids[15] may be added to the Nafion membrane in order to increase the water uptake from the humidified gas feed, while employment of transparent, hydrophobic layers at the PV front may reduce the condensation issues. The former allows the use of lower humidity feeds while the latter enables high humidity feeds.

The current density of 12 mA cm^{-2} (equivalent to a peak STH efficiency of 14%) achieved with the PIM device compares favorably to other reported vapor-fed devices (solid lines in Fig. 5).[7,16,17] In fact, the initial current density approaches those of highly-efficient, fully-integrated, liquid devices (dashed lines in Fig. 5),[4–6] and is higher after just 30 min of operation. The LBNL 2 device,[19] where the PV is completely encapsulated by a protective epoxy, is the only integrated, liquid device in Fig. 5 showing a constant performance. The stability enhancement of the vapor-fed PIM device becomes obvious, when the results are compared to the liquid-fed PIM (black lines in Fig. 5), presented recently by the authors.[18] The current density is much more stable, even when only the 180 h displayed in Fig. 4 are compared. The significant reductions in the effective concentration of water, in the vapor-fed system relative to

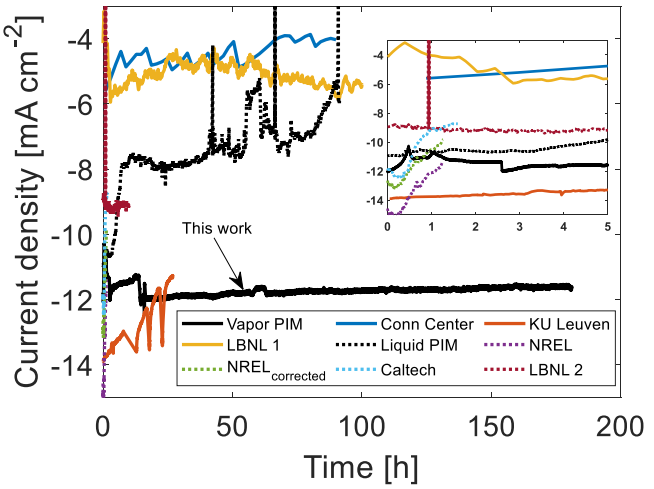

Figure 5. Performance comparison of the vapor-fed PIM device with recently reported solar hydrogen devices under 1 sun illumination intensity. Current measurements of Conn Center[16] and KU Leuven[17] were cycled through dark and light cycles, causing the spikes in the current. The current density of the device from KU Leuven[17] is based on the PV size (3.54 cm^2) while the electrolyzer is slightly larger (4 cm^2). The authors note that the devices from Conn Center[16] and KU Leuven[17] physically separate the PV and electrolyzer components, while the former is using a seawater vapor feed and the latter employs earth-abundant catalysts. Data from LBNL 1[7] and Caltech[6] were smoothed to remove noise and increase visibility. Results from NREL[5] were rescaled (green trace) based on their reported, maximum efficiency as previously suggested by Caltech.[6] Original NREL data is shown in purple. Previous data from the authors is labeled as liquid PIM[18] and from Walczak et al. as LBNL 2.[19]

bulk-aqueous devices, result in milder operating conditions for the PV, as it limits the rate of corrosion reactions occurring at PV defect sites. The outcome is an appreciable enhancement in device stability and longevity. The authors note that a comparison of STH efficiencies is arguably more valuable, as it includes possible losses reflected in the faradaic efficiency. Reduced faradaic efficiencies may stem from a variety of sources, such as parasitic corrosion reactions or increased hydrogen crossover. However, due to the absence of faradaic efficiency data for all the devices being compared, current density was used as the figure-of-merit for these comparisons.

Conclusion

Stability is one of the main issues prohibiting commercial applications for PEC devices. This manuscript communicates the demonstration of a fully-integrated, vapor-fed water splitting device operating at a peak STH efficiency of 14% during in-lab and on-sun testing, under varying operating conditions. During the course of 1000 h, we observed only minor, irreversible PV degradation, highlighting the potential utility of employing water-vapor anodes to extend PEC device lifetimes. However, outdoor conditions made it more difficult to sustain the peak efficiencies. In addition, we show that outdoor PEC tests can be significantly influenced by their surroundings, as white walls and reflective pipes may effectively concentrate the light intensity when compared to radiation data from a local weather station. Therefore, we recommend using a reference cell to measure the effective light intensity during outdoor experiments.

Acknowledgments

The authors thank Nemanja Danilovic, Frances Houle, Jason Cooper, David Larson, Jeffrey Beeman, and Ian Sharp for their helpful insights and aid with the experimental setup. The authors gratefully acknowledge research support from the Joint Center for Artificial Photosynthesis (JCAP), a DOE Energy Innovation Hub, supported through the Office of Science of the U.S. Department of Energy under Award Number DE-SC0004993.

ORCID

Tobias A. Kistler https://orcid.org/0000-0001-6458-8024
Min Young Um https://orcid.org/0000-0001-5174-3232
Peter Agbo https://orcid.org/0000-0003-3066-4791

References

1. E. L. Miller, *Energy Environ. Sci.*, **8**, 2809 (2015).
2. M. Carmo, D. L. Fritz, J. Mergel, and D. Stolten, *Int. J. Hydrogen Energy*, **38**, 4901 (2013).
3. D. Jing, L. Guo, L. Zhao, X. Zhang, H. Liu, M. Li, S. Shen, G. Liu, X. Hu, and X. Zhang, *Int. J. Hydrogen Energy*, **35**, 7087 (2010).
4. M. M. May, H.-J. Lewerenz, D. Lackner, F. Dimroth, and T. Hannappel, *Nat. Commun.*, **6**, 8286 (2015).
5. J. L. Young, M. A. Steiner, H. Döscher, R. M. France, J. A. Turner, and T. G. Deutsch, *Nat. Energy*, **2**, 453 (2017).
6. W.-H. Cheng, M. H. Richter, M. M. May, J. Ohlmann, D. Lackner, F. Dimroth, T. Hannappel, H. A. Atwater, and H.-J. Lewerenz, *ACS Energy Lett.*, **3**, 1795 (2018).
7. T. A. Kistler, D. Larson, K. Walczak, P. Agbo, I. D. Sharp, A. Z. Weber, and N. Danilovic, *J. Electrochem. Soc.*, **166**, H3020 (2019).
8. S. Tembhurne, F. Nandjou, and S. Haussener, *Nat. Energy*, **4**, 399 (2019).
9. C. Xiang, Y. Chen, and N. S. Lewis, *Energy Environ. Sci.*, **6**, 3713 (2013).
10. J. M. Spurgeon and N. S. Lewis, *Energy Environ. Sci.*, **4**, 2993 (2011).
11. Khaselev and Turner, *Science*, **280**, 425 (1998).
12. F. Dionigi, P. C. K. Vesborg, T. Pedersen, O. Hansen, S. Dahl, A. Xiong, K. Maeda, K. Domen, and I. Chorkendorff, *Energy Environ. Sci.*, **4**, 2937 (2011).
13. J. Rongé et al., *RSC Adv.*, **4**, 29286 (2014).
14. E. A. Chandross, *Science*, **344**, 469 (2014).
15. J. Rongé, T. Bosserez, L. Huguenin, M. Dumortier, S. Haussener, and J. A. Martens, *Oil Gas Sci. Technol.*, **70**, 863 (2015).
16. S. Kumari, R. Turner White, B. Kumar, and J. M. Spurgeon, *Energy Environ. Sci.*, **9**, 1725 (2016).
17. G. Heremans, C. Trompoukis, N. Daems, T. Bosserez, I. F. J. Vankelecom, J. A. Martens, and J. Rongé, *Sustainable Energy Fuels*, **1**, 2061 (2017).
18. T. A. Kistler, N. Danilovic, and P. Agbo, *J. Electrochem. Soc.*, **166**, H656 (2019).
19. K. A. Walczak, G. Segev, D. M. Larson, J. W. Beeman, F. A. Houle, and I. D. Sharp, *Adv. Energy Mater.*, **7**, 1602791 (2017).
20. J. Rongé, D. Nijs, S. Kerkhofs, K. Masschaele, and J. A. Martens, *Phys. Chem. Chem. Phys.*, **15**, 9315 (2013).
21. C. Ampelli, G. Centi, R. Passalacqua, and S. Perathoner, *Energy Environ. Sci.*, **3**, 292 (2010).
22. B. Seger and P. V. Kamat, *J. Phys. Chem. C*, **113**, 18946 (2009).
23. M. A. Modestino, M. Dumortier, S. M. H. Hashemi, S. Haussener, C. Moser, and D. Psaltis, *Lab Chip*, **15**, 2287 (2015).
24. W. J. C. Vijselaar, P. Perez-Rodriguez, P. J. Westerik, R. M. Tiggelaar, A. H. M. Smets, H. Gardeniers, and J. Huskens, *Adv. Energy Mater.*, **9**, 1803548 (2019).
25. T. A. Kistler and P. Agbo, *APL Mater.*, **8**, 31107 (2020).